Lasers in Manufacturing Conference 2023

Numerical model of laser energy attenuation due to interaction of the laser beam with stream of powder particles in Direct Energy Deposition

Mohammad Sattari[a,*], Martin Luckabauer[b], Gert-willem R.B.E. Römer[a]

[a]*Chair of Laser Processing, department of Mechanics of Solids, Surfaces & Systems (MS3), Faculty of Engineering Technology, University of Twente, Drienerlolaan 5, 7522 NB Enschede, The Netherlands*
[b]*Chair of Production Technology, department of Mechanics of Solids, Surfaces & Systems (MS3), Faculty of Engineering Technology, University of Twente, Drienerlolaan 5, 7522 NB Enschede, The Netherlands*

Abstract

In laser direct energy deposition (L-DED), interactions between laser beam and powder particles significantly affect the laser-induced melt pool in the substrate. This study introduces a novel laser energy attenuation model, addressing absorption and reflection of laser energy by powder particles. The model calculates attenuated laser beam intensity profiles in the focal spot and incorporates them into a high-fidelity thermo-fluid model for L-DED. This comprehensive model considers multiple physical phenomena, including temperature and angle-dependent absorption, powder particle stream, particle-fluid interactions, temperature-dependent properties, buoyancy effects, thermal expansion, phase transitions, evaporation, solidification, and Marangoni flow driven by temperature and element-dependent surface tension. The total attenuated laser power , as well as the attenuated beam intensity profiles are determined for both circular and square uniform laser beams, examining their impacts on melt pool behavior. Comparisons between numerical and experimental fusion zone morphologies reveal that neglecting laser energy attenuation results in significant deviations in fusion zone dimensions, underscoring the importance of incorporating laser energy attenuation in L-DED models.

Keywords: Laser direct energy deposition, Laser beam intensity profile, Laser energy attenuation, Thermo-fluid modeling;

1. Introduction

In Laser-assisted powder-based Direct Energy Deposition (L-DED), the laser beam induces a met pool in the substrate, into which a stream of powder particles, propelled by a gas through a nozzle, is injected, see Fig. 1. Both the powder stream and laser beam are moved in the same direction during the deposition process. Additionally, a shielding gas is employed to protect the melt pool against oxidation [1].
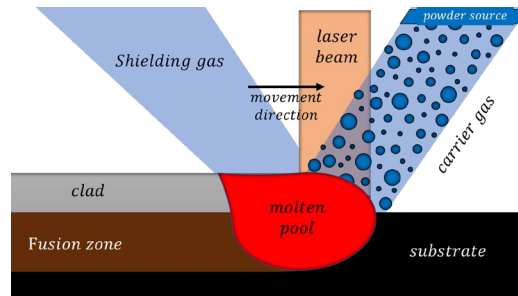
Fig. 1. Schematic representation of laser-assisted powder-based direct energy deposition (DED).

In L-DED, powder particles interact with the laser beam within the gas region prior to entering the melt pool [1]. During their travel time through the laser beam, the powder absorbs, reflects and diffracts part of the laser radiation leading not only to a total attenuation of the laser power, but also to a local attenuation of the laser intensity profile in the focal spot on the substrate [1]. While analyzing this phenomenon, transmission of laser light through the particles can be neglected, as the particle size is much larger than the optical penetration depth of the typical laser wavelength used.

In order to accurately model the L-DED process as a whole, it is crucial to account for the attenuation of laser power and the intensity profile of the laser beam due to the stream of powder particles. Neglecting this phenomenon can lead to significant discrepancies between simulations and experimental results. Relevant literature covers studies on the modeling of the attenuation of laser energy in L-DED, both analytically and numerically. Analytical models [2]–[13] are generally faster in computation compared to numerical models. However, analytical models are based on simplifications, such as excluding particle rebound and the particle velocity distribution, which reduce the reliability of the simulation results. Numerical models [14]–[16] offer higher levels of accuracy and detail. Nevertheless, their computational requirements are considerably heavier, making them impractical for integration into larger numerical models such as high-fidelity multiphase thermo-fluid L-DED simulations.

This paper presents a novel model for laser energy attenuation, due to the powder stream, that allows to study the effects of the powder stream on both the total laser power loss and the local attenuation of the beam intensity profile. The model takes not only into account specific characteristics of the powder stream but also incorporates the shadowing effect of the laser beam caused by particles bouncing off the smooth surface of the substrate. This study integrates the laser energy attenuation model into a high-fidelity thermo-fluid model developed using computational fluid dynamics (CFD). To validate the model, the dimensions of the solidified fusion zone generated by a circular uniform intensity profile are compared with experimental results.

2. Modeling

This section outlines the modeling efforts necessary to capture the intricate aspects of the L-DED process. First, the modeling of the powder stream is discussed, emphasizing the powder particle distribution and dynamics. Subsequently, the heat transfer mechanism during the interaction between the laser beam and powder particles is presented. Following that, the laser energy attenuation model is introduced, providing insight into the reduction of laser energy and attenuation in laser intensity profile. Lastly, a brief introduction of the thermo-fluid model, which integrates the laser energy attenuation model, is presented.

2.1. Powder Stream

To model the dynamics of individual particles, the Discrete Element Method (DEM) [17] is employed. In this approach, it is assumed that all particles travel at the same velocity. Therefore, the influence of gravity and drag force exerted by the transport gas on the particles is neglected. In addition, it is assumed that particles do not interact—i.e. particles do not collide.

Fig. 2a shows the particle diameter (d) and size distribution (D) of the powder used, obtained through sieving measurements. The rate of particles in the powder stream, denoted as $\dot{n}_i$ having a diameter of d_i can be calculated using,

$$\dot{n}_i = \frac{\dot{m}}{\rho V_i} \frac{D_i}{100},\tag{1}$$

where $\dot{m}$ is the powder mass addition rate (in this case, 2.5 g/min), ρ is the material density of the powder, and D_i and V_i represent the particle size distribution (expressed as a percentage) and volume, respectively, for particles with a diameter of d_i. The sum of the $\dot{n}_i$ values provides the total rate of particles in the stream. It is assumed that the total particle rate shows a normal distribution across the cross-sectional plane of the powder stream [18]. Additionally, the experimentally measured diameter of the powder stream (here, 3.2 mm) is considered to be half of the real diameter. Under this assumption, the powder rate at the radius of the stream is $1/e^2$ of the maximum powder rate in the center of the stream [9]. Fig. 2b depicts the resulting distribution.
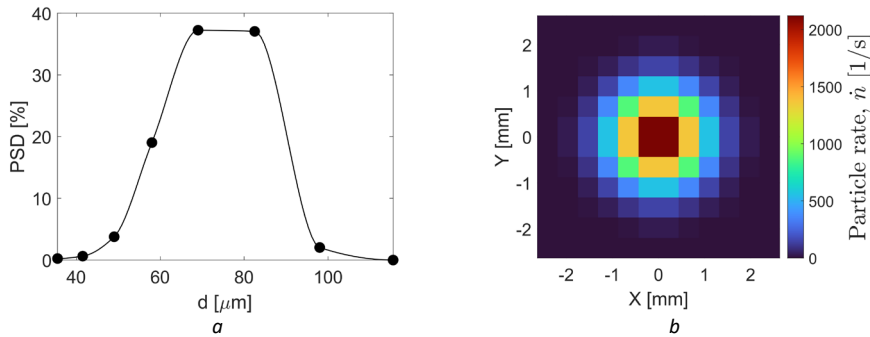

Fig. 2. a) Measured particle size distribution, using the sieving technique; b) Transverse cross-section of the designed powder stream used in the simulations.

2.2. Heat Transfer in Laser-Powder Interaction

The temperature change of a particle resulting from its interaction with the laser beam can be calculated by the lumped-capacitance method as [19],

$$\rho V c_p(T) \frac{dT}{dt} = \alpha(T) I_L(x,y,z,t) \frac{A}{4} - h_w A(T - T_0) - \varepsilon_s \sigma A\left(T^4 - T_0{}^4\right),\tag{2}$$

where c_p is the specific heat of powder material, t is time, T denotes temperature of the particle, α represents the laser energy absorption coefficient of the particle, I_L denotes the spatiotemporal laser beam intensity profile, A represents the surface area of the particle, h_w is the heat convection coefficient, ε_s denotes the emissivity of the particle's surface, σ represents the Stefan-Boltzmann constant, and T_0 is the surrounding temperature. It is assumed that the laser energy absorption coefficient, α, depends on temperature. The temperature-dependent absorption coefficient is calculated using a general Fresnel model, which is extensively described in [20] and [21]. Fig. 3 shows the corresponding temperature dependence of

the absorption coefficient. However, the effect of the angle of incidence of the laser beam on the particle on the absorption coefficient is disregarded. Consequently, particles are considered as two-dimensional projected circles that are perpendicular to the laser beam. Under this assumption, the diffraction of the laser ray is neglected, and a laser ray is reflected upon interacting with the particle.
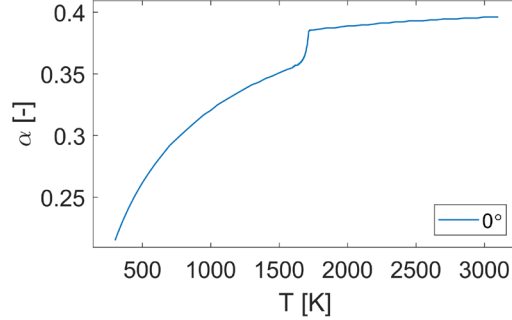

Fig. 3. Laser absorption coefficient, α, as function of temperature, of an austenitic stainless steel for Yb:YAG radiation.

2.3. Laser Energy Attenuation

As shown in Fig. 4, two scenarios can occur when a laser beam and a powder stream intersect above and on the surface of the substrate. That is, in the first scenario (Fig. 4a), the "horizontal diameter" of the powder stream equaling $d_s/sin(\theta_s)$, is larger than the diameter of the laser beam, d_L. Here, θ_s denotes the angle between the powder stream and the horizonal. In this scenario, particles that strike the surface of the substrate ahead (right-side) of the laser beam (in the light blue region in Fig. 4a) bounce off the substrate and subsequently enter the laser beam (in the green region). On the other hand, particles that are irradiated by the laser beam before reaching the surface (in the dark blue region) can either enter the melt pool or collide with the resolidified surface behind (left-side of) the laser beam, without bouncing back into the laser beam.

When a particle positioned at point H hits the smooth solid surface at point O, it is assumed that it undergoes an elastic collision. In that case, no friction is present between the particle and the surface. As a result of this collision, the particle rebounds and travels to point H'. The difference in height between points H and H', indicated by ΔH, is the result of the kinetic energy that is lost during the collision. This energy loss is determined by the restitution coefficient, denoted as e_p, which characterizes the elasticity of the contact between the steel particle and the steel surface. Taking into account the given assumptions and considering the geometric relationship between the parameters depicted in Fig. 4a, the minimum required lengths of the powder stream (L_s), and laser (L_L) can be determined as,

$$L_s = \overline{OH} + L_1 + L_2 = \frac{[d_L \sin(\theta_s)+d_s].[3+\cos(2\theta_s)]+2d_s}{2 \sin(2\theta_s)}, \qquad (3)$$

$$L_L = \overline{OH} \sin(\theta_s) = \frac{d_L \sin(\theta_s)+2d_s}{2 \cos(\theta_s)}, \qquad (4)$$

where $L_1 = \frac{d_s}{2} cot(\theta_s)$, and $L_2 = \frac{d_L}{2} cos(\theta_s)$.

a) Scenario i: $d_s/sin(\theta_s) \geq d_L$ b) Scenario ii: $d_s/sin(\theta_s) < d_L$
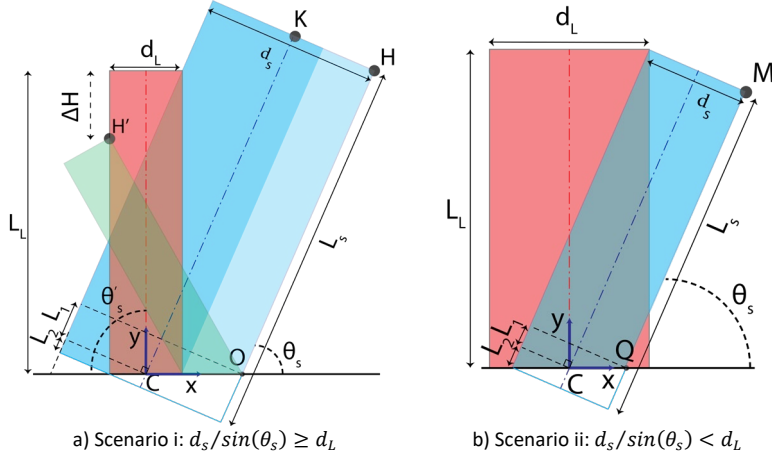
Fig. 4. Two scenarios of laser beam (red) and powder stream (blue) intersection over and on the substrate surface. In the first scenario, the green zone represents the area where particles bounce back towards the laser beam.

Conversely, when the horizontal diameter of the powder stream is shorter than the diameter of the laser beam, as indicated in Fig. 4b, the diameter of the powder flow cylinder is smaller than the diameter of the laser beam. Therefore, all particles enter the melt pool without bouncing from the surface of the substrate. In this scenario,

$$L_s = \overline{OM} + L_1 + L_2 = \frac{d_L \sin(\theta_s) + d_s}{\sin(2\theta_s)}, \tag{5}$$

$$L_L = L_s \sin(\theta_s) = \frac{d_L \sin(\theta_s) + d_s}{2 \cos(\theta_s)}, \tag{6}$$

where $L_1 = L_2 = \frac{d_s}{2} \cot(\theta_s)$.

Based on the experimental values of the flow rate of the carrier gas and the diameter of the powder stream on the surface, the velocity of powder particles, v_p, is found to equal to 5 m/s, which is typical for the powder velocity in L-DED. Accordingly, the time required to model particles within the powder stream cylinder is,

$$t_s = \frac{L_s}{v_p}; \tag{7}$$

Hence, the quantity of particles modeled with a diameter of d_i, can be ascertained through,

$$n_i = round\big(v_p \dot{n}_i t_s\big), \tag{8}$$

In order to determine the location of particles within the powder stream (defined as powder particles distributed in a cylinder), a random selection is employed for the azimuth and axial distances, while for the radial distance a normal distribution of particles is chosen with a standard deviation of $d_s/4$. In order to incorporate the bouncing behavior of powder particles, the particles within the light blue region are duplicated and mirrored along the vertical axis that passes through the collision point of the particle with the surface of the substrate. Their height is recalculated based on the restitution coefficient.

The laser beam intensity profile is characterized by the total power (scalar) and a normalized power density profile that specifies the distribution of the total power within the intensity profile. To calculate the attenuated intensity profile, a configuration of the interaction of laser beam and particle stream is modeled. To consider

the random positions of particles in the powder stream, the modeled laser-powder configuration is repeated. The number of times each point in the laser beam profile is shaded, is recorded. Next, the resulting attenuated power density profile is obtained by averaging the power density values over iterations. The attenuation rate is determined by using the difference between the sum of the power density of points in the initial profile and that of the attenuated profile.

2.4. Thermo-Fluid Model

The above laser attenuation model, is incorporated into a three-dimensional high-fidelity thermo-fluid model, extensively described in [21]. The thermo-fluid model employs the Finite Volume Method (FVM) and Volume of Fluid (VoF) technique to solve equations related to mass, momentum, energy conservation, as well as advection of the free surface. Various coupled physical phenomena are considered, including temperature and incidence angle dependency of the laser energy absorption at the surface of the substrate, multiple reflections of laser rays, interactions between particles and the fluid, temperature-dependent material properties, buoyancy effects, thermal expansion, phase transitions, evaporation, solidification, and the occurrence of Marangoni flow driven by temperature and element-dependent surface tension.

3. Experimental Setup

A Yb:YAG disk laser (TruDisk 10001, TRUMPF SE + Co. KG, Germany) with a 1030 nm wavelength is used to irradiate the substrate's surface perpendicularly. The beam is transported though and optical fiber and focused into a 1.2 mm diameter focal spot, showing a uniform circular intensity profile (Top Hat), as shown in Fig. 5b, [20], [22]. As a substrate material a 316L stainless steel plate is used. The powder material is also 316L stainless steel. The powder is supplied by a powder feeder. The powder is injected into the melt pool by argon gas through a 1.5 mm diameter off-axis powder nozzle at a 70° angle to the horizontal. Processing parameters are set to 600 W laser power, 5 mm/s traverse speed, and a powder feeding rate of 2.5 g/min. After the experiment, samples are cut, polished, and etched using a solution of 100 mL HCl, 100 mL H_2O, and 10 mL NHO_3 at 310 K for digital imaging [20], [22].

4. Result and Discussion

### 4.1. Laser Energy Attenuation

Fig. 5a presents an isometric view of the modeled laser beam, powder stream, and bouncing particles. Within this figure, the gray region represents the location of particles entering the melt pool. Fig. 5b displays the unattenuated laser beam power density profile, showcasing the profile when there is no interaction with particles. Moving on to Fig. 5c, a single simulation instance illustrates a group of particles (dark blue) that cause shading on the Top Hat profile. The locations of particles and their impact on the beam profile are replicated a thousand times. Subsequently, the average attenuated intensity profile is computed. Fig. 5d exhibits the resulting average attenuated profile. Notably, as depicted in this figure, the powder stream unsurprisingly induces a line-shaped area with reduced intensity at the front of the laser profile. The corresponding total attenuation of the laser beam is calculated to be 14.6%.
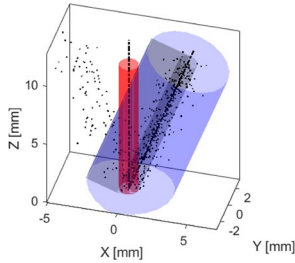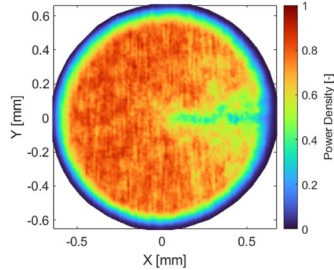
a) isometric (simulated) view of the laser beam (red) and powder flow (blue), containing particles (black).
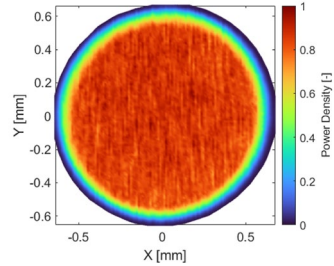
b) contour plot of the measured, unattenuated, normalized laser beam power density profile
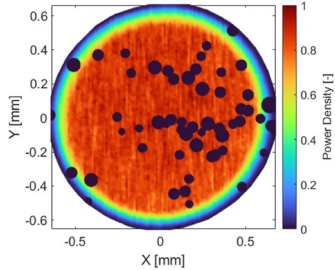
c) contour plot of an instance of the simulated normalized intensity profile, shaded by powder particles (dark blue).

d) simulated normalized averaged shaded profile after a thousand iterations.

Fig. 5. The underlying principles of the proposed laser energy attenuation model for the powder addition rate of 2.5 g/min, and particle velocity of 5 m/s.

Next, the effect of powder shading on three other laser beam intensity profiles—annular, square, and U-shaped uniform profiles as shown in Fig. 6 (top row), is simulated. Fig. 5d and the bottom row of Fig. 6 substantiate the crucial role of incorporating the bouncing of powder particles in models designed for laser beam shaping applications. Across all profiles, the attenuation of the laser beam's front side is observed to be more pronounced in comparison to the back side. Of course this implies that intensity profiles which exhibit lower intensities at their front side suffer less from powder particle shielding than profiles showing higher intensity at the front side. This assertion is especially pronounced for the U-shaped (or horse-shoe shaped) profile, see the most right graphs in Fig. 6.

4.2. Effect of powder shading on melt pool and heat affected zone and comparison to experiments

To investigate the influence of laser energy attenuation, the transverse cross-sections of L-DED thermo-fluid simulations are compared to experimental counterparts. Two scenarios are considered. In the first scenario, the laser beam power and intensity profile are analyzed without any attenuation, while in the second scenario, the beam power and intensity profiles are examined with attenuation. Fig. 7a presents a comparison between the optical microscopy image of a transverse cross-section from the experimental deposition track (left) and a simulated transverse cross-section of the track formed by an unattenuated laser beam (right). Additionally, Fig. 7b compares the experimental and numerical cross-sections of a deposited track using an attenuated laser beam. The resolidified region is clearly visible in the experimental cross-sections, while the white band in the simulated cross-sections represents the fusion zone boundary.

It is found that neglecting the attenuation of the laser beam leads to a significant simulation error of 15.5% in the depth of the melt pool, as shown in Fig. 7a. Furthermore, in this case, the errors in height and width are

negligible, with values of 1% and 2.3%, respectively. However, when laser energy attenuation is considered, the simulation error in the depth of the melt pool decreases to 5.8% (Fig. 7b). Similarly, negligible height and width error values are 2.8% and 1.4%, respectively. These findings highlight the significance of accounting for laser beam attenuation to improve the accuracy of melt pool characterization in laser metal deposition processes.
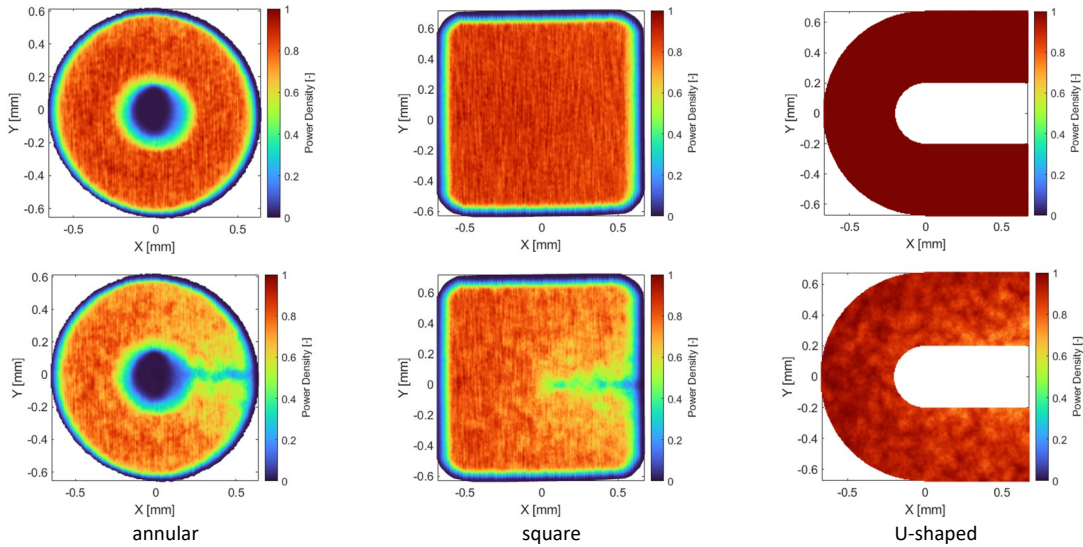

Fig. 6. (Top row) contour plots of the unattenuated of laser beam intensity profiles and (bottom row) contour plots of attenuated power density profiles, demonstrating the effect of particle bouncing.

a) No laser energy attenuation   b) Attenuated laser power and intensity profile
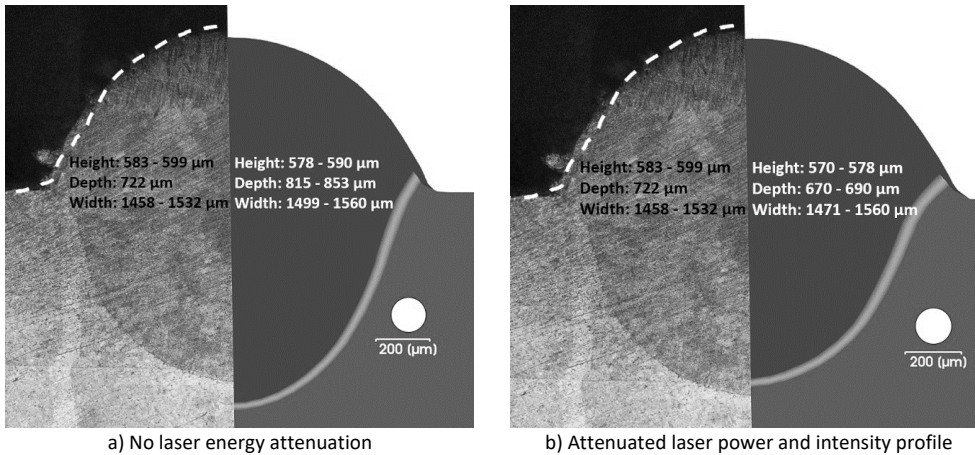
Fig. 7. Comparison of the experimental and numerical transverse cross-sections for the circular uniform laser beam with a power of 600 W, powder addition rate of 2.5 g/min, and particle velocity of 5 m/s.

5. Conclusion

This paper introduced a novel model that incorporates the shading, i.e., local attenuation, of the laser beam intensity profile caused by the stream of powder particles in powder-based laser-assisted direct energy

deposition (L-DED). The model also accounts for shading effects caused by particles bouncing off the surface. From simulation results is was found that the powder stream significantly attenuates the front of the laser beam intensity profile. The laser energy attenuation model was integrated into a high-fidelity thermo-fluid model. Comparing the dimensions of the deposited track induced by an unattenuated Top-Hat laser profile to those of an attenuated one, it was observed that the dimensions of the track and the resolidified zone in the substrate are strongly influenced by the shading effect of the powder stream. Experimental results, involving cross-sections of the deposited tracks using a Yb:YAG laser source with stainless steel as both powder and substrate material, demonstrated that the simulation results incorporating the attenuation model accurately predict the dimensions of the resolidified zone with a depth error of 5.8%. Conversely, when the attenuation model is not considered, the depth of the fusion zone was predicted with 15.5% error. In both cases, the errors in width and height were negligible.

Acknowledgements

References

[1]   G. Piscopo, E. Atzeni, A. Saboori, and A. Salmi, "An Overview of the Process Mechanisms in the Laser Powder Directed Energy Deposition," *Applied Sciences*, vol. 13, no. 1, p. 117, Dec. 2022, doi: 10.3390/app13010117.

[2]   A. J. Pinkerton, "An analytical model of beam attenuation and powder heating during coaxial laser direct metal deposition," *J. Phys. D: Appl. Phys.*, vol. 40, no. 23, pp. 7323–7334, Dec. 2007, doi: 10.1088/0022-3727/40/23/012.

[3]   A. J. Pinkerton, R. Moat, K. Shah, L. Li, M. Preuss, and P. J. Withers, "A verified model of laser direct metal deposition using an analytical enthalpy balance method," in *International Congress on Applications of Lasers & Electro-Optics*, Orlando, Florida, USA: Laser Institute of America, 2007, p. 1806. doi: 10.2351/1.5061038.

[4]   I. Tabernero, A. Lamikiz, S. Martínez, E. Ukar, and L. N. López De Lacalle, "Modelling of energy attenuation due to powder flow-laser beam interaction during laser cladding process," *Journal of Materials Processing Technology*, vol. 212, no. 2, pp. 516–522, Feb. 2012, doi: 10.1016/j.jmatprotec.2011.10.019.

[5]   J. Wang, Z. Zhang, F. Han, S. Chen, and W. Ying, "Modeling of laser power attenuation by powder particles for laser solid forming," *Procedia CIRP*, vol. 95, pp. 42–47, 2020, doi: 10.1016/j.procir.2020.02.286.

[6]   C. Vundru, R. Singh, W. Yan, and S. Karagadde, "A comprehensive analytical-computational model of laser directed energy deposition to predict deposition geometry and integrity for sustainable repair," *International Journal of Mechanical Sciences*, vol. 211, p. 106790, Dec. 2021, doi: 10.1016/j.ijmecsci.2021.106790.

[7]   N. Sobhanieh, J. Akbari, and M. Moradi, "A new method for calculating laser intensity distribution on workpiece surface in laser-directed energy deposition process by considering powder stream distribution and laser attenuation," *Int J Adv Manuf Technol*, vol. 121, no. 1–2, pp. 337–348, Jul. 2022, doi: 10.1007/s00170-022-09301-1.

[8]   W. Jiazhu, T. Liu, H. Chen, F. Li, H. Wei, and Y. Zhang, "Simulation of laser attenuation and heat transport during direct metal deposition considering beam profile," *Journal of Materials Processing Technology*, vol. 270, pp. 92–105, Aug. 2019, doi: 10.1016/j.jmatprotec.2019.02.021.

[9]   Y. Huang, M. B. Khamesee, and E. Toyserkani, "A comprehensive analytical model for laser powder-fed additive manufacturing," *Additive Manufacturing*, vol. 12, pp. 90–99, Oct. 2016, doi: 10.1016/j.addma.2016.07.001.

[10]   Y.-L. Huang, J. Liu, N.-H. Ma, and J.-G. Li, "Three-dimensional analytical model on laser-powder interaction during laser cladding," *Journal of Laser Applications*, vol. 18, no. 1, pp. 42–46, Feb. 2006, doi: 10.2351/1.2164476.

[11] F. Brückner, D. Lepski, and E. Beyer, "Modeling the Influence of Process Parameters and Additional Heat Sources on Residual Stresses in Laser Cladding," *J Therm Spray Tech*, vol. 16, no. 3, pp. 355–373, Aug. 2007, doi: 10.1007/s11666-007-9026-7.

[12] H. Liu and Y. Zhou, "An interaction model for laser and powder in wide-beam laser cladding," *Int J Adv Manuf Technol*, vol. 112, no. 1–2, pp. 15–23, Jan. 2021, doi: 10.1007/s00170-020-06330-6.

[13] Y. Fu, A. Loredo, B. Martin, and A. B. Vannes, "A theoretical model for laser and powder particles interaction during laser cladding," *Journal of Materials Processing Technology*, vol. 128, no. 1–3, pp. 106–112, Oct. 2002, doi: 10.1016/S0924-0136(02)00433-8.

[14] J. Ibarra-Medina and A. J. Pinkerton, "A CFD model of the laser, coaxial powder stream and substrate interaction in laser cladding," *Physics Procedia*, vol. 5, pp. 337–346, 2010, doi: 10.1016/j.phpro.2010.08.060.

[15] W. Devesse, D. De Baere, and P. Guillaume, "Modeling of laser beam and powder flow interaction in laser cladding using ray-tracing," *Journal of Laser Applications*, vol. 27, no. S2, p. S29208, Feb. 2015, doi: 10.2351/1.4906394.

[16] X. Guan and Y. F. Zhao, "Numerical modeling of coaxial powder stream in laser-powder-based Directed Energy Deposition process," *Additive Manufacturing*, vol. 34, p. 101226, Aug. 2020, doi: 10.1016/j.addma.2020.101226.

[17] M. Bayat *et al.*, "On the role of the powder stream on the heat and fluid flow conditions during Directed Energy Deposition of maraging steel—Multiphysics modeling and experimental validation," *Additive Manufacturing*, vol. 43, p. 102021, Jul. 2021, doi: 10.1016/j.addma.2021.102021.

[18] S. M. Thompson, L. Bian, N. Shamsaei, and A. Yadollahi, "An overview of Direct Laser Deposition for additive manufacturing; Part I: Transport phenomena, modeling and diagnostics," *Additive Manufacturing*, vol. 8, pp. 36–62, Oct. 2015, doi: 10.1016/j.addma.2015.07.001.

[19] A. Aggarwal, S. Patel, A. R. Vinod, and A. Kumar, "An integrated Eulerian-Lagrangian-Eulerian investigation of coaxial gas-powder flow and intensified particle-melt interaction in directed energy deposition process," *International Journal of Thermal Sciences*, vol. 166, p. 106963, Aug. 2021, doi: 10.1016/j.ijthermalsci.2021.106963.

[20] A. Ebrahimi *et al.*, "The influence of laser characteristics on internal flow behaviour in laser melting of metallic substrates," *Materials & Design*, vol. 214, p. 110385, Feb. 2022, doi: 10.1016/j.matdes.2022.110385.

[21] M. Sattari, A. Ebrahimi, M. Luckabauer, and G. R. B. E. Römer, "Laser beam shaping in directed energy deposition additive manufacturing: computational modeling and experimental validation," *Under preparation*.

[22] S. J. L. Bremer, M. Luckabauer, and G. R. B. E. Römer, "Laser intensity profile as a means to steer microstructure of deposited tracks in Directed Energy Deposition," *Materials & Design*, vol. 227, p. 111725, Mar. 2023, doi: 10.1016/j.matdes.2023.111725.